Friction **12**(4): 726–744 (2024)
https://doi.org/10.1007/s40544-023-0797-8
ISSN 2223-7690
CN 10-1237/TH

RESEARCH ARTICLE

Eco-friendly polysaccharide coatings for antifouling and drag-reduction and potential application for marine devices

Hao YANG[1], Liguo QIN[1,*], Wenhui ZHAO[2], Fagla Jules MAWIGNON[1], Hui GUO[3], Yongkang WU[1], Yali ZHANG[2,*], Guangneng DONG[1]

[1] *Key Laboratory of Education Ministry for Modern Design and Rotor-Bearing System, Institute of Design Science and Basic Components, School of Mechanical Engineering, Xi'an Jiaotong University, Xi'an 710049, China*

[2] *Key Laboratory of Biomedical Information of Ministry of Education, School of Life Science and Technology, Xi'an Jiaotong University, Xi'an 710049, China*

[3] *Department of Endocrinology, First Affiliated Hospital of Medical College, Xi'an Jiaotong University, Xi'an 710061, China*

Received: 15 April 2023 / Revised: 02 June 2023 / Accepted: 02 July 2023

Abstract: Traditional antifouling agents usually have a certain toxic effect on marine environments and non-target organisms. In this study, *Dictyophora indusiata* polysaccharide (DIP) was applied as a natural antifouling surface modifier to prepare the surface coating for marine antifouling. Three DIP coatings were prepared: *D. indusiata* spore polysaccharide (DISP), *D. indusiata* volva polysaccharide (DIVP), and *D. indusiata* embryonic body polysaccharide (DIEP). The antifouling, tribological, and anticorrosion behavior of the coatings were examined. Results revealed that the three kinds of DIP coatings had excellent antifouling properties, which could effectively prevent the adhesion of Chlorella and the attachment of water-based and oily stains on the surface. Additionally, the coatings showed great mechanical stability and could maintain an extremely low coefficient of friction (COF < 0.05) after continuous wear. The drag reduction rate of the coated surfaces reached 5%, showing a powerful lubrication performance. Furthermore, the DIP coatings presented an outstanding corrosion resistance, where the equivalent circuit impedances were 4–9 orders of magnitude higher than the control groups. This research showed a promising prospect of surface coating fabrication with DIP for marine devices to achieve the purpose of antifouling and drag reduction.

Keywords: *Dictyophora indusiata* polysaccharide (DIP) coating; antifouling; anticorrosion; lubrication and drag reduction

1 Introduction

For several decades, marine fouling has seriously troubled ships and other underwater equipment. Fouling organisms growing on submerged surfaces can promote deterioration and increase shipping resistance, resulting in high fuel consumption and large maintenance costs [1, 2]. Moreover, high fuel consumption would produce more greenhouse gases to accelerate global warming and fouling organisms would sail along the ships to damage local ecosystems. Therefore, great focus should be emphasized on the antifouling coatings for submerged surfaces to reduce economic losses and avoid environmental pollution problems.

The fouling attachment process on the submerged surfaces can be described in three stages [3–5]. First, organic and inorganic molecules such as proteins are adsorbed onto the ship surface, changing the physical and chemical properties of the surface and forming a conditioning film. Then, the nutrients on this film will attract bacteria, which are attached to the surface

* Corresponding author: Liguo QIN, E-mail: liguoqin@xjtu.edu.cn; Yali ZHANG, E-mail: yar.lee@xjtu.edu.cn

through interaction with organic macromolecules to form a biofilm. Subsequently, algae, barnacles, and other large fouling organisms will further attach to the biofilm, eventually forming macroscopic fouling.

Apparently, the most effective protection method against fouling is to prevent the early adhesion of microorganisms. For this prevention, the use of chemical paint is currently widely popular. However, traditional antifouling agents containing tributyltin (TBT) are not specific and are highly toxic to aquatic organisms. Meanwhile, their substitutes, such as cuprous oxide (Cu_2O), cuprous thiocyanate (CuSCN), and other copper compounds, although far less toxic than TBT, still have a negative impact on the growth of some non-target marine organisms [4]. Therefore, research hotspots should be emphasized with more environment-friendly and efficient antifouling agents for marine surface coatings. Creatures in nature have evolved surfaces with excellent antifouling performance. Inspired by these natural antifouling surfaces, six bionic strategies for preparing antifouling coatings are revealed [3]: (i) micro/nanostructured surfaces; (ii) natural antifoulants; (iii) mucus-like hydrogels; (iv) slippery liquid infused porous surfaces (SLIPS); (v) dynamic surfaces; (vi) zwitterionic coatings.

In 2011, Wong's group [6] first proposed the concept of slippery lubricant infused surfaces (SLIS), which employed both the capillary force and van der Waals force to attract per fluorinated lubricant in the stable surface [7, 8]. The lubricants used to fabricate SLIS mainly include silicone oil, vegetable oil, mineral oil, ionic liquid, Perfluoropolyether [9], etc., and extensive research has been carried out in the fields of antifouling, anticorrosion, anti-icing, and transparency. The most common method to prepare SLIS is to inject lubricating oil with low surface energy on the superhydrophobic surface. However, it would complicate the preparation process and expend the cost if using ionic liquid and per fluorinated lubricating oil as the injection liquid. In addition, per fluorinated lubricating oil also pollutes the environment to a great extent. Lubricants such as silicone, plant, and mineral oils have relatively low costs but could negatively impact the environment. The research on SLIS in recent years could be mainly divided into the following directions [9]: (i) design of a highly stable structure, which could control the release of lubricating fluid and effectively resist external interference; (ii) introduction of functional substances into the system for better performance; (iii) research new surface modifier materials to improve performance; (iv) change the connection mode between the surface modifier and the constructed substrate from intermolecular force to chemical bond for improving the stability. For the third direction, there are research on chemical modification of natural substances (such as vegetable oil) to synthesize antibacterial substances [4], but their chemical modification operations are complex. Furthermore, research on environmental-friendly antifouling coatings using oleic acid and methyl oleate is also very popular [10, 11] but still harmful to non-target organisms. Bio-friendly surface modifiers, especially natural ones, possess great research value and prospects. The mixed tungsten disulfide (WS_2) microparticles were reported to be immobilized with hydrophobic SiO_2 nanoparticles on the sponge by non-toxic polydimethylsiloxane (PDMS) [12]. The obtained PDMS@SiO_2@WS_2 sponge showed excellent oil adsorption capacity and oil/water selectivity with a separation efficiency of over 99.85%. However, when subjected to the complex marine biofoulings, the modified sponge could not maintain stable superhydrophobicity with a water contact angle over 150°. However, research on hydrophilic macromolecular coatings for biological fouling prevention, especially for inhibiting microbial adhesion, is also extensive. Park et al. [13] applied chitosan nanofilm as a coating layer on the inner wall of medical silicone tubes to adsorb anti-inflammatory and antibacterial substances for achieving bacterial inhibition. Polysaccharide extracted from *Dictyophora indusiata* (DIP) was reported as a good bacteriostasis [14]. Therefore, we assumed that DIP could effectively prevent the formation of biofilm composed of bacteria before the macroscopic fouling. Similarly, Pradal et al. [15] successfully covalently grafted pectin onto the surface of PDMS at its reducing end through a reductive amination reaction, providing a reference for our design of DIP grafting onto PDMS. Meanwhile, there have been numerous reports on the use of polysaccharides as surface modifiers to improve surface lubrication performance. In 2011, McNamee et al. [16] synthesized a dextran silane coupling agent to graft polydextran

onto silicon oxide wafers, achieving friction-reducing effect. However, the polydextrose film on hard silicon wafers was prone to the damage during service and failed to achieve long-term service. Clementine modified PDMS with pectin through a covalent grafting method. The hydration of the pectin layer resulted in a stable and tough lubricating property on the surface. Bourouis et al. [17] conducted a detailed analysis of the study of polysaccharides combined with fats as a food lubricant. Also, Ji et al. [18] used a variety of common edible polysaccharides (maltose dextrin, corn starch, etc.) to test the dynamic tribological properties of dairy drinks, resulting in an average COF from 0.05 to 0.5. However, the COF values were still much higher than the ultra-low friction range (<0.05).

In our research, DIP was used as an antifouling surface modifier, and PDMS as a coating substrate. Firstly, a transparent substrate was prepared through the condensation reaction of PDMS with curing agent addition. Subsequently, the substrate was cleaned by plasma, and a large number of hydroxyl groups were excited on the surface. Then, the DIP molecules were planted onto the microporous structure of PDMS and combined with hydroxyl to form a uniform DIP coating. The physical and chemical properties of the DIP coating surface were studied, and a series of characterization tests were designed to verify the performance of the coating in terms of antifouling, corrosion resistance, lubrication, and drag reduction. Results showed that our study provides distinct inspirations for developing effective antifouling and anticorrosion coatings with environment-friendly natural antifouling agents.

2 Experimental procedure

2.1 Materials

PDMS precursor was purchased from Dow Corning Co., Ltd., USA. The cellulose, ethanol, and deionized water were purchased from China National Medicines Co. Ltd., China. All chemical reagents are of analytical grade and were used without further purification. The fresh *D. indusiata* young basidicarpus, water- and oil-based stamps were purchased online.

2.2 Preparation of DIP antifouling surfaces

2.2.1 *Preparation of DIP solutions*

The fresh *D. indusiata* young basidicarpus was washed with deionized water and then disassembled into spore, core and cell wall to extract DIP. These three parts were dried in the oven for 45 min at 60 °C (Lichen Instrument Equipment Co., Ltd., Shanghai, China). The spore, core, and cell wall were named DISP, DIEP, and DIVP, respectively. The extraction methods of the three polysaccharides were the same, so only DIEP was described below. After full grinding, the DIEP powder was added to pure water at a mass ratio 1:1 to make a mixed slurry. Then, ultrasonic treatment was conducted at 40 kHz and 40 °C for 15 min in the ultrasonic cleaning machine (Buck Ultrasonic Technology Co., Ltd., Jinan, China). The obtained mixture was centrifuged at 4,000 r/min for 15 min with a centrifuge (Miqi Instrument Equipment Co., Ltd., Changsha, China), added cellulose, and then kept at room temperature for 3 h. Centrifugation was repeated twice, and the supernatant was extracted. To separate the effective substances from impurities, ethanol sedimentation was applied to obtain a DIEP solution.

2.2.2 *Preparation of DIP coating surfaces*

The preparation process of DIP coating surfaces is shown in Fig. 1. The PDMS base and curing agent were mixed at a ratio of 10:1 in a beaker, then stirred for 3 min with the magnetic stirrer (Yuezhong Instrument Equipment Co., Ltd., Shanghai, China) to be fully mixed. After that, the mixture was applied onto the clean Q235 steel substrate until solidification. The three kinds of DIP solutions were used as the lubricant, and a concentration of 1% was set for the coatings. The PDMS film was cleaned with a plasma cleaner (Jiabuli Electronic Equipment Co., Ltd., Nanjing, China) before immersion in the polysaccharide solution. Afterward, each DIP solution was dropped onto the surface of PDMS films, soaked for 24 h, and then the excess solution was scraped off to form a uniform and stable sugar film on the surface. Each group contained more than 21 identical and independent samples so that each subsequent characterization experiment could be repeated at least three times to approve the reproducibility of the data. Finally, all

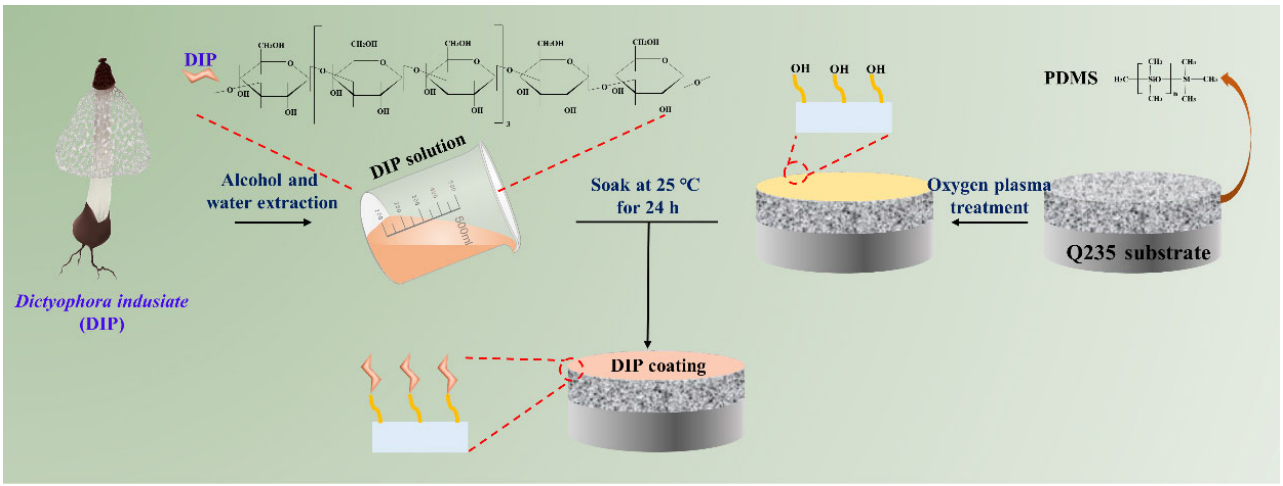

Fig. 1 Preparation process of DIP coating surfaces.

samples were stored at room temperature for further study.

The grafting mechanism of DIP onto the surface of PDMS is a covalent branching chemical reaction. The surface hydroxylated PDMS surface was first treated with oxygen plasma to achieve exposure of –OH and –CH_2OH groups. With the help of hydroxyl groups, the diffusion process of DIP aqueous solution on the surface of PDMS became faster due to strong intermolecular interactions. Because of the bonding process, the two layers of atoms were gradually pushed toward the interface. They penetrated each other, forming a reliable bond at the interface, greatly improving the efficiency of DIP covalent grafting onto PDMS. The surface of PDMS grafted with DIP could be well characterized through methods such as atomic force microscopy (AFM), Fourier Transform infrared spectroscopy (FTIR), and wettability measurement [19].

2.3 Characterization

The static contact angle (CA) of pure water (5 μL) on the sample surfaces was measured using a contact angle system (JC2000D2A, POWEREACH, China) equipped with a tilting platform. Through the sessile drop method, the reported data were the calculated average value of five recordings at different places on samples.

The surface morphology of samples was captured by a field emission scanning electron microscope (MAIA3 LMH, USA) and an atomic force microscope (SPM-9700HT, Japan).

FTIR spectra results were recorded from fourier transform infrared spectroscope (Nicolet iS50, USA) equipped with an MVP-PRO attenuated total reflection (ATR) unit (diamond crystal, 45° angle of incidence) and a KBr beam splitter. A scanning range of 550–4,000 cm^{-1} with a resolution of 4 cm^{-1} and average over 100 scans were used. The baseline correction of FTIR spectra was performed using the concave rubber band correction method with the OPUS software (Version 8.5, Bruker Optics Incorporation, USA).

For mechanical strength characterization, samples were cut into the dumbbell shape with an overall thickness of 1 mm and a width of 4 mm in the middle, and the tensile measurement was performed with the double-column desktop universal material testing machine (INSTRON 5965, USA). Under the action of uniaxial tension, PDMS goes through elastic deformation until fracture. Since the clamping part of the tensile testing machine has a convex texture, protective stickers were pasted on both ends of each sample during the test to prevent the sample from being damaged at the clamping part during sample placement and subsequent stretching. During clamping, the end of the test section of the sample was aligned with the edge of the fixture to ensure that the initial distance of repeated experiments was consistent. The load accuracy was set to 0.5%. In order to ensure the accuracy of the experimental data, each group of experiments was repeated 3 times. Then the obtained stress-strain curve was analyzed to evaluate the elongation at break and the elastic modulus.

2.4 Tribological, antifouling, and anticorrosion behavior

A tribometer (UMT-2, Center for Tribology Co., USA) was selected to measure the anti-friction efficiency of DIP coatings at ambient temperature under water-lubricated conditions. A GCr15 ball with a diameter of 9.5 mm was installed in the clamp of the tribometer as the upper sample. Figure 2(a) shows a schematic diagram of the ball-on-disc test. Fukushima et al. [20] employed the computational fluid dynamics (CFD) method to obtain optimum parameters, where 20 MPa was chosen as the average contact pressure to simplify the experimental design. Therefore, for a pressure of 20 MPa, the load was calculated to 2 N during the sliding shearing test via the Hertz contact theory. The corresponding sliding speed and time were adjusted to 0.036 m/s and 30 min, respectively. The coefficient of friction (COF) was recorded, and all tests were repeated at least three times at room temperature.

As shown in Fig. 2(b), the electrochemical corrosion test of bare alloy (Q235), bare PDMS, and three kinds of DIP coatings was conducted through the three-electrode workstation of CHI electrochemical analyzer (CHI660E). The samples were immersed in a 3.5% NaCl solution to simulate the corrosion behavior of the marine environment. The test frequency was 10^{-2}–10^{5} Hz. The reference electrode was a saturated calomel electrode; the auxiliary electrode was a platinum sheet; the working electrode was Q235 metal with coating. The size of the metal block was 1 cm^2, and the thickness was about 5 mm. Insulated PDMS wrapped both sides of Q235, and the thickness of the PDMS film was about 2 mm. The electrolyte solution was 3.5% NaCl, and the samples were soaked for 0.5 h before measurement. The impedance, corrosion current density, corrosion potential, and other parameters of different samples were obtained by the Nyquist diagram, Byrd diagram, and Tafel curves based on the measurement results of electrochemical impedance spectroscopy (EIS) for determining the corrosion resistance of the coating.

In Fig. 2(c), Chlorella, a unicellular alga distributing worldwide, was selected to test the anti-adhesion ability. The mixture was poured into a transparent glass beaker after mixing pure water, chlorella seeds, and culture medium in a mass ratio of 50:2:1. When the room temperature was kept at 25 °C, the mixed liquid was kept in the natural light environment and stirred every 6 h. After 5 d, the color gradually changed to green, and then it was used as an antifouling test solution rich in Chlorella.

3 Results and discussion

3.1 Basic characterization of DIPs and DIP coatings

3.1.1 *FTIR spectra and viscosity of DIPs*

ATR-FTIR measurement (Fig. 3) was performed for further confirmation of the chemical groups and

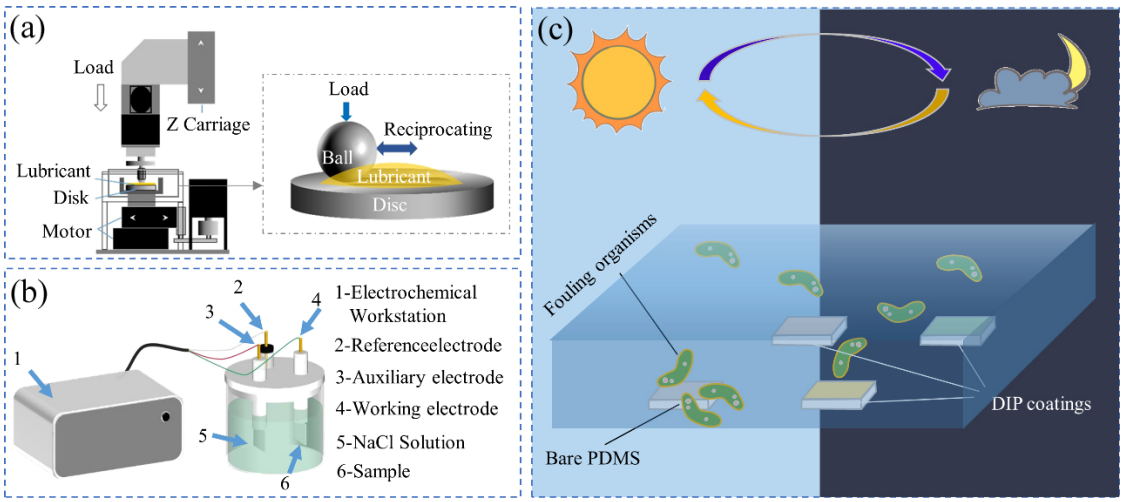

Fig. 2 Design of characterization tests: (a) schematic diagram of ball-on-disc test, (b) three-electrode test system, and (c) Chlorella adhesion test.

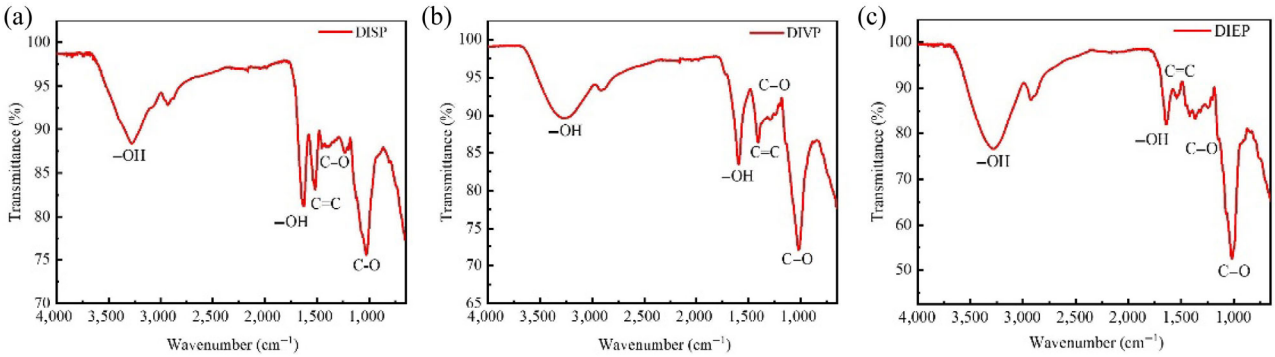

Fig. 3 FTIR spectra of DIPs: (a) DISP, (b) DIVP, and (c) DIEP.

structures of the three polysaccharides DISP, DIEP, and DIVP. At wave number 3,200–3,300 cm^{-1}, a large number of hydroxyl (–OH) functional groups were determined for the three DIPs. From the light transmittance, it could be seen that the hydroxyl content of DIVP was higher, while the hydroxyl content of the other two was approximately the same. Near 1,600 cm^{-1}, both DIVP and DIEP showed narrow hydroxyl group peaks again; However, the carbon double bond (C=C) group was determined at 1,600 cm^{-1} by DISP; DIVP and DIEP determined the C=C group at 1,520–1,530 cm^{-1} wave number. In addition, the carbon-oxygen single bond (C–O) groups of the three polysaccharides were determined at the wave numbers 1,400 cm^{-1} and 1,000 cm^{-1}. The existence of hydrophilic groups such as hydroxyl had a decisive influence on the preparation and service of subsequent DIP coatings.

Fluid viscosity is an important solution migration property. Its measurements usually include vibration, a falling body, rotation, capillary, and optical methods. It can measure the viscosity of pure liquid or gas phase. The viscosity of present antifouling lubricants is too high or too low to prevent the attachment of fouling organisms [21, 22]. The high viscosity is not conducive to the exudation of the polysaccharide lubricant and the spreading of the polysaccharide lubricant on the coating surface under the service conditions. The low viscosity would lead to the poor adhesion of the polysaccharide lubricant to the PDMS substrate and would easily slide off the surface with water under external disturbances. In addition, in the field of engine wear reduction, engines generally use oil to achieve the purpose of anti-friction lubrication in service. To ensure the normal lubrication of each friction pair, properly reducing the oil viscosity could reduce the friction loss of components under fluid lubrication [23, 24]. Similarly, the polysaccharide lubricant coated on the PDMS substrate could prevent the substrate's friction loss while ensuring the lubrication performance.

Figure 4 shows the dynamic viscosities of three polysaccharide solutions at shear rates of 1, 50, and 100 /s, tested at room temperature. The concentration of three polysaccharide solutions was 17 mol/L. The difference in viscosity of different polysaccharide solutions could be attributed to the different intermolecular and intramolecular forces and the degree of intermolecular hydrogen bonds. It could

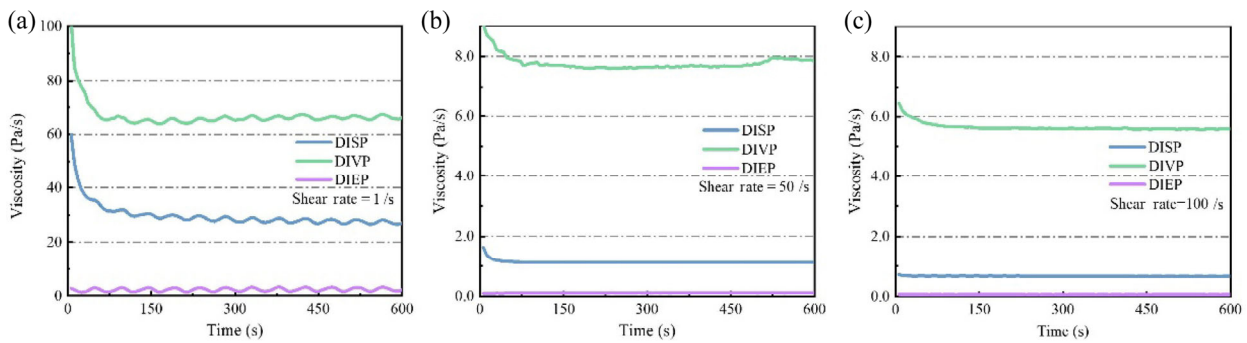

Fig. 4 Dynamic viscosities of DIPs at different shear rates: (a) 1 /s, (b) 50 /s, and (c) 100 /s.

be seen from Fig. 6 that under different shear rates, the viscosities of the DIPs solutions ranged from high to low from DIVP, DISP, to DIEP. With the increase in shear rate, the viscosities decreased. When the shear rate increased from 1 to 50 /s, the viscosity of DISP and DIVP decreased from 30 and 65 to 1.2 Pa/s and 7.9 Pa/s, respectively; while from 50 to 100 /s, the viscosity of both decreased slightly. The viscosity of DIEP was slightly higher than 0 Pa/s at the three shear rates, and it changed little with the shear rate.

3.1.2 Mechanical properties and wettability of DIP coatings

The tensile test of each group of samples was repeated three times. The elastic modulus of the sample was obtained from the slope of the stress-strain curve. The average value of the three data groups was measured to obtain the average elastic modulus of the material. Similarly, for the elongation at break (the maximum tensile deformation rate when the sample breaks), three groups of samples were also measured for each sample, and the average value was taken. The stress-strain curve of each sample is shown in Figs. 5(a)–5(d), the average elastic modulus and average elongation at break are shown in Fig 5(e), and Fig. 5(f) is the tensile diagram of the samples.

Previous results revealed that coating surface modifiers could change the compressive strengths and modulus of elasticity with different kinds and densities [25]. The toughness of the composites can be considerably increased by coating nano-HA with EGMP before failure. While, with the addition of BIS-EGMP, the ductile behavior disappeared, and the composites showed brittle behavior. It is concluded that the influence of hydrogen bonding or electrostatic interactions of the phosphate groups of the surface modifiers was studied in this work and represented a valuable basis for tailoring new composites usable as biomaterials in coating construction. FTIR spectra of DIPs were studied in the former section, and the obvious differences in hydrogen bonding of DIPs were observed, which explained the different mechanical performances of coatings. Therefore the mechanical properties of different DIP coatings should be studied, and the results are shown in Table 1. The elastic modulus of the three DIP coatings were higher than that of bare PDMS. The elastic modulus of PDMS was 0.2589 MPa. And the elastic modulus of the DISP, DIVP, and DIEP coatings were 0.5019, 0.6486, and 0.4787 MPa, respectively. The result revealed that DIP coatings had smaller deformation and stronger resistance to elastic deformation than bare PDMS, and DIVP coating showed the highest elastic modulus and the strongest resistance to elastic deformation.

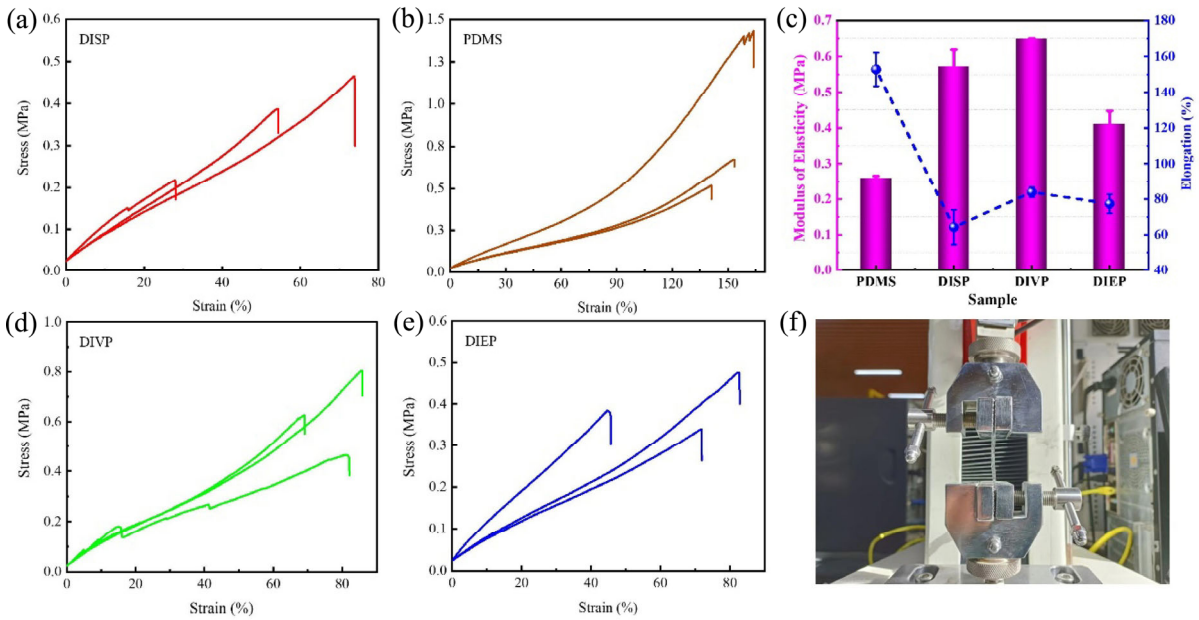

Fig. 5 Stress-strain curves of (a) PDMS, (b) DISP, (c) DIVP, and (d) DIEP; (e) the mechanical properties of samples; (f) tensile test diagram.

Table 1 Mechanical properties of different coatings.

Sample	Tensile strength (MPa)	Modulus of elasticity (MPa)	Elongation (%)
Bare PDMS	0.76±0.33	0.26±0.01	152.89±9.29
DISP	0.31±0.01	0.50±0.05	74.60±7.33
DIVP	0.55±0.13	0.65±0.01	83.96±1.89
DIEP	0.45±0.06	0.48±0.05	85.49±1.96

From the maximum tensile deformation rate at fracture, it was clear that the elongation at break of the three polysaccharide coatings (DISP, DIVP, and DIEP were 74.60%, 83.96%, and 85.49%, respectively) was significantly lower than that of PDMS (152.89%). Three DIPs endow the coatings with different mechanical properties and are a little weaker than bare PDMS coating owing to the modified effects of DIPs. The same tensile adhesion test based on modified ASTM C633–13 standards on HVOF, HAS, and WCN coated surfaces were performed to test the mechanical performance [26], where those coatings displayed relatively lower stress values (less than 0.23 MPa), indicating that the DIP coatings can still resist the deformation under external force well.

The coating's wettability, surface energy, and elastic modulus play important roles in anti-adhesion performance. Studying these basic characteristics of materials can help researchers understand the antifouling mechanism of the coating, which is conducive to the preparation of bionic antifouling coating. Wettability is the ability of the liquid to contact a solid surface, which is determined by the intermolecular force between liquid and solid surface. CA measurement is the most commonly used method to determine wettability. When a liquid droplet contacts a solid in the air, there will be three phases: solid, liquid, and gas. The static CA is defined as the tangent angle of the gas–liquid interface at the intersection of three phases. If the CA is less than 10°, the surface is defined as super hydrophilic; If it is between 10° and 90°, it is hydrophilic; If it is between 90° and 150°, it is a hydrophobic surface; If it exceeds 150°, it is superhydrophobic surface. The average CAs collected for each sample are displayed in Fig. 6. Different from many common antifouling coatings (hydrophobic), all three DIP coatings showed a certain degree of hydrophilicity, and even the CA

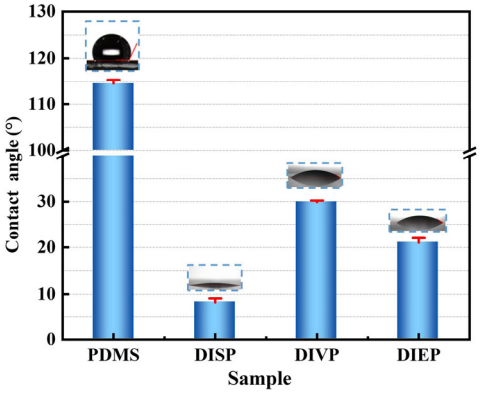

Fig. 6 Static CA of four coatings.

of the DISP coating was reduced below 10°, showing super hydrophilicity. Similarly, Wang et al. [27] prepared a hydrophilic synthetic cellulose film on a polyvinylidene fluoride (PVDF) surface through the enzymatic method, endowing the coating with excellent antifouling and antibacterial activity. However, the surface contact angle decreased to about 40°, much higher than the CA of DIP coatings. Compared with bare PDMS, the CAs of PDMS surfaces grafted DIP were significantly reduced, and the polarity was enhanced. The static CA varies within the range of 8°–29°, indicating the superior hydrophilicity endowed to these DIP surfaces. This behavior may be related to the large number of hydrophilic groups observed by FTIR in DIPs, confirming that DIPs were grafted onto PDMS. The analysis of FTIR spectra of DIPs in Section 3.1.1 gave us the explanation of hydrophilicity.

3.1.3 *Surface morphology of DIP coatings*

As shown in Fig. 7, SEM and AFM were conducted to observe the surface micromorphology of the different coatings. Figs. 7(a2)–7(d2) showed the SEM results, and Figs. 7(a1)–7(d1) displayed the AFM results of the four coatings. The images of the same coating obtained by the two methods were consistent. Before observation with SEM, it was necessary to spray Pt on the sample coating with low conductivity. During the spraying process, it was found that when the scanning voltage was too high or the scanning time was too long, the sugar film on the coating surface was easy to be damaged. Therefore, the combination of AFM imaging results could better reflect the micromorphology of different coatings. By comparison,

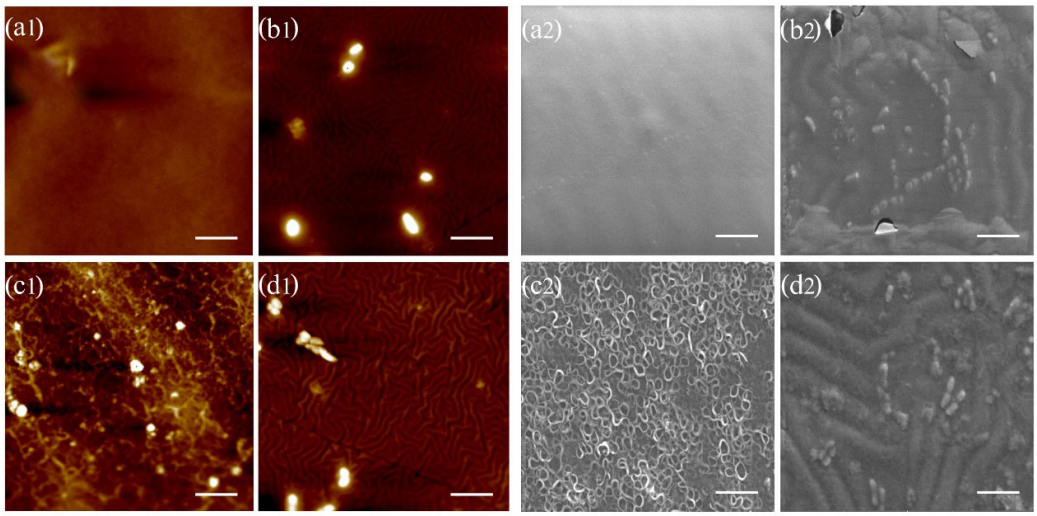

Fig. 7 Surface morphologies of (a) bare PDMS, (b) DISP coating, (c) DIVP coating, and (d) DIEP coating, where 1 for AFM and 2 for SEM. All scale bars are 5 μm

the bare PDMS showed smooth surface morphology, and the three DIP coatings displayed a DIP film on PDMS. The surface morphologies of DISP and DIEP were in the shape of water ripples, and there were aggregations of granular polysaccharide molecules. The AFM images of samples described in Fig. 8 revealed the changes in surface morphology after DIP grafting. The roughness values of the grafted DIP coatings were significantly higher than that of bare PDMS, indicating that the surface is filled with a large number of polysaccharide polymer chains. The height of the aggregation area of polysaccharide molecules protruded significantly as bright spots. Unlike DISP and DIEP, molecules on DIVP were much denser and ringed all over the PDMS substrate.

Figure 8 shows the samples' surface element energy spectrum and the peak value corresponding to the element content. Apart from a small amount of sprayed Pt, the bare PDMS contained a large amount of Si elements and C and O elements. However, the three DIP coatings only exposed a smaller amount of Si elements than C and O elements, revealing that the DIP films were uniform and covered the PDMS substrates well.

The difference between bare PDMS and DIP coatings could be easily seen through the three-dimensional morphology of the four coatings observed by AFM (Fig. 9). It could be found that the bare PDMS surface was quite smooth, and the height change within 30 μm was only about 10 nm. However, the height changes of DISP, DIVP, and DIEP coatings were 550, 75, and 350 nm, respectively, which indicated that the

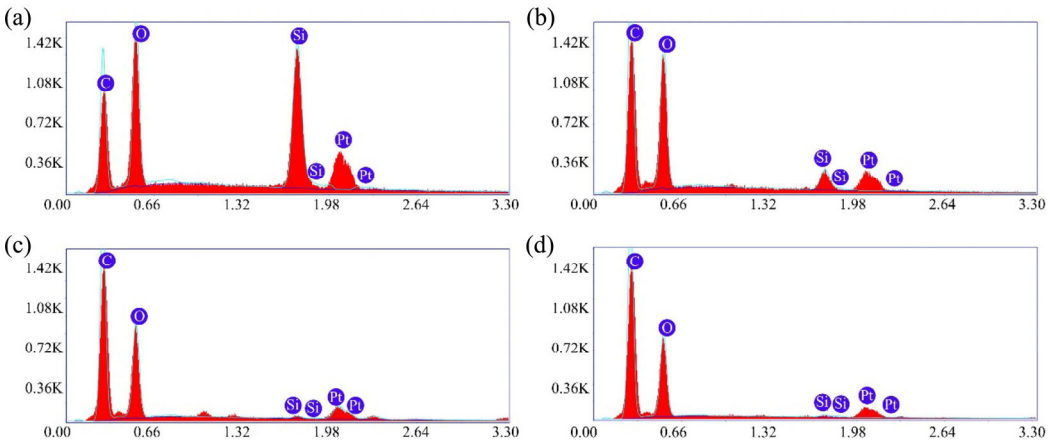

Fig. 8 Element energy spectra of (a) bare PDMS, (b) DISP coating, (c) DIVP coating, and (d) DIEP coating.

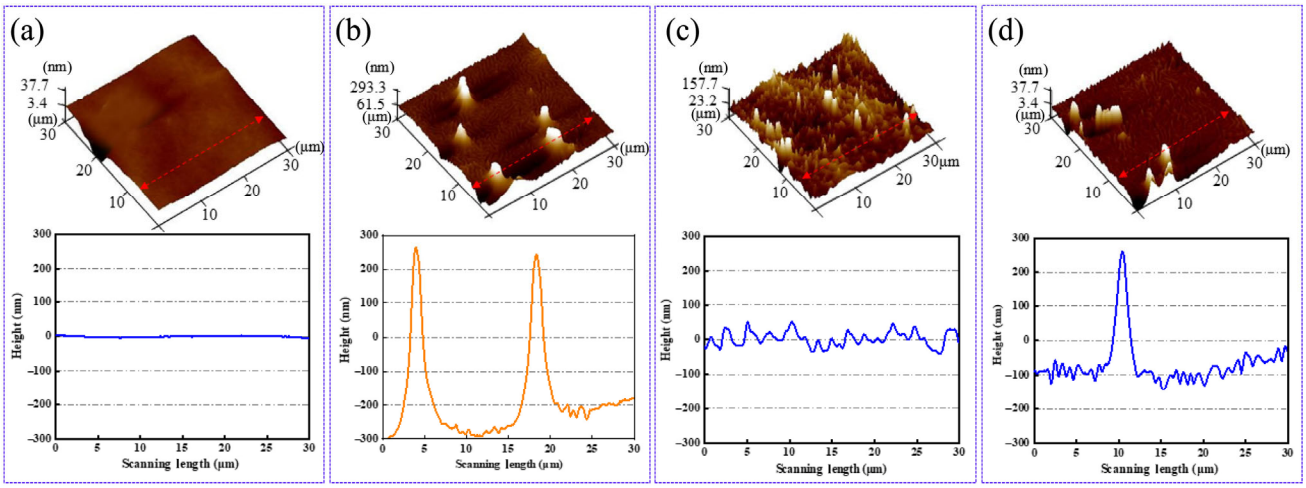

Fig. 9 Three-dimensional AFM morphology and height change diagrams of (a) bare PDMS, (b) DISP coating, (c) DIVP coating, and (d) DIEP coating.

growth of DIP films showed a huge influence on the morphology of the coatings. Different morphologies of surface modifiers could also cause changes in the polymer matrix network and lead to mechanical properties variation, consistent with the results of tensile tests.

3.2 Slippery behavior and drag reduction performance

The relationship between the COF and the frequency for the kinds of DIPs was determined in Fig. 10. The average COF values obtained from different samples and under different working conditions are listed in Table 2. In Fig. 10(a), the COF values of the three DIP coatings greatly fluctuated, and the average COFs of DISP, DIVP, and DIEP were 0.030, 0.062, and 0.044, respectively. Compared with the COF of PDMS (1.082) at the same frequency in Fig. 10(d), there was still a gap of two orders of magnitude. With the increase in frequency, we could see in Figs. 10(b) and 10(c) that the COF of DIP coating was lower than that under 1 Hz working conditions. The average COFs of DISP, DIVP, and DIEP were 0.025, 0.054, and 0.030 at 2 Hz, and 0.032, 0.047, and 0.033 at 4 Hz, respectively. It can also be seen that under the same working conditions, all three DIP coatings showed excellent slippery properties. When the frequency increased, the COF of the same coating changed little, indicating that when the external frequency was within a certain range, the lubrication characteristics of the coating were similar.

Table 2 Average COF of different coatings in water lubrication.

Sample	Frequency (Hz)	Average COF
DISP	1	0.030
	2	0.025
	4	0.032
DIVP	1	0.062
	2	0.054
	4	0.047
DIEP	1	0.044
	2	0.030
	4	0.033
Bare PDMS	1	1.082
	2	1.121
	4	1.056

The COF ranged from 0.02 to 0.05 (quite low). At the same time, it could be found that the COFs of the DIP coatings were very stable compared with bare PDMS, even if the wear process was maintained for about 30 min, indicating that the wear resistance of DIP coatings was quite strong.

The resistance of a ship during navigation can be seen as the tangential and normal forces from the water acting on the ship's surface, also known as friction resistance and pressure resistance [28]. The adhesion of fouling organisms on the bottom of the ship increased the friction resistance of the ship during navigation. In this test, the drag reduction platform independently built in the laboratory was used to

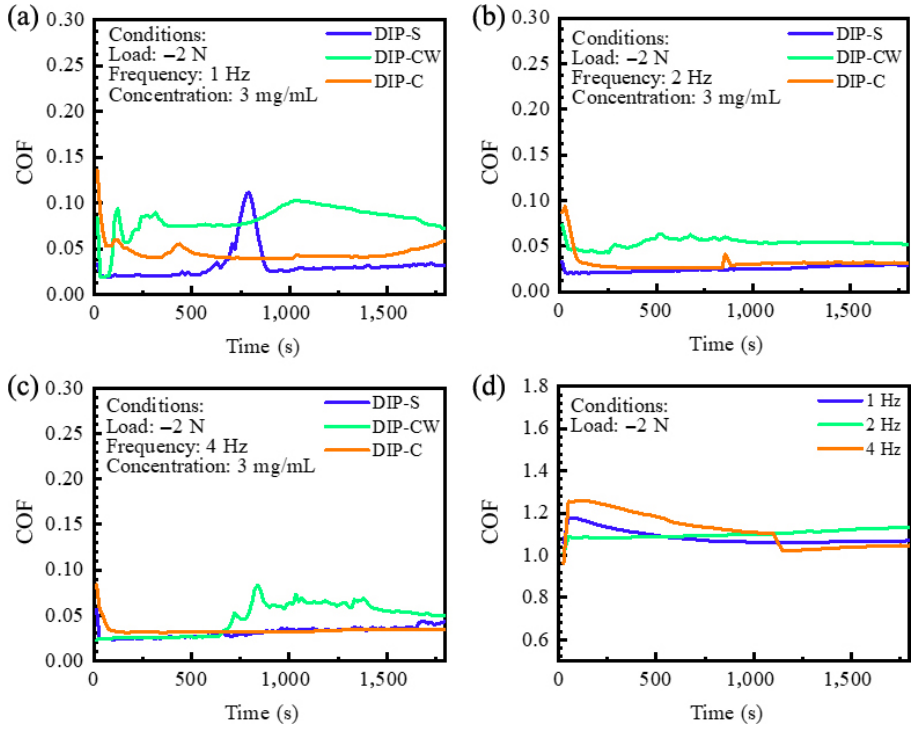

Fig. 10 COFs of the DIP coatings at the frequencies of (a) 1 Hz, (b) 2 Hz, and (c) 4 Hz, and (d) COFs of PDMS under 2 N and water lubrication.

simulate the service conditions of four kinds of coatings at different flow velocities. With bare PDMS as the control group, the drag reduction rate (R) of three kinds of DIP coatings was defined as

$$R = \frac{F_{\mathrm{PDMS}} - F_{\mathrm{DIP}}}{F_{\mathrm{PDMS}}} \times 100\% \quad (1)$$

where, F_{PDMS} and F_{DIP} are the forces on bare PDMS or on PDMS covered by DIP along the water flow direction, respectively.

The flow rate was set as 0.07, 0.08, 0.09, and 0.1 m/s. Each sample was measured three times at each flow rate and the average value of R was calculated. The force values are recorded in Table 3, and the result of R on DIP coatings is shown in Fig. 11.

It can be seen from Fig. 11 that the drag reduction rate of DISP and DIEP coatings increased with the increase of water flow rate, from 3.38% and 3.76% to 5.72% and 5.05%, respectively, while the drag reduction rate of DIVP coating decreased with the increase of water flow rate, from 4.51% to 3.03%. In general, the drag reduction rates of the coatings obtained under laboratory conditions were between 2% and 6%, which could bring considerable economic benefits and

Table 3 Force on each sample along flow direction at different flow velocities v.

v (m/s)	F_{DISP} (N)	F_{DIVP} (N)	F_{DIEP} (N)	F_{PDMS} (N)
0.0702	0.2574	0.2540	0.2561	0.2662
0.0814	0.2630	0.2642	0.2620	0.2745
0.0906	0.2665	0.2711	0.2672	0.2790
0.1006	0.2801	0.2882	0.2825	0.2970

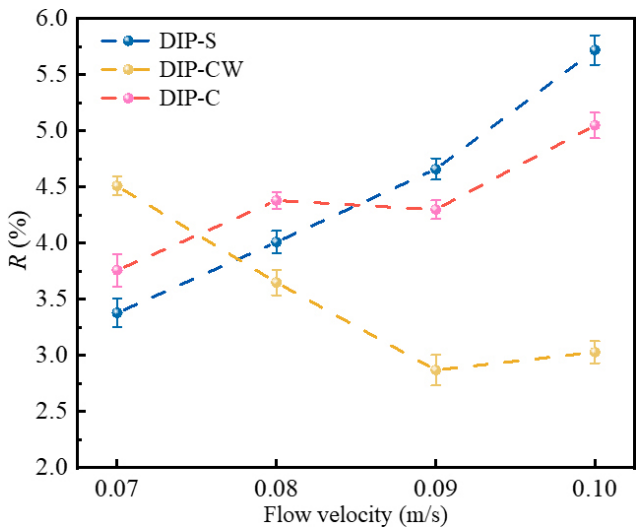

Fig. 11 Drag reduction rate of three DIP coatings under different flow velocities.

be significant to environmental protection. Therefore, the result of the drag reduction experiment had a certain guiding significance for the actual drag reduction applications. The existence of abundant hydrophilic groups in DIPs has been observed from the FTIR spectra, which enables it possible to endow the coating with the ability to form a hydration barrier [29], thus making the coating have excellent low friction performance and drag reduction performance.

3.3 Evaluation of anticorrosion performance

The anticorrosion performance is a significant property of surfaces for fabricating the surfaces facing harsh and complicated marine environment [30]. Electrochemical corrosion in the sea can be mainly divided into concentration cell effect of oxygen, corrosion of different metals, corrosion caused by oxide skin, and corrosion caused by stray current. The corrosion of ships in the sea caused damage to the ship hull, reduced its service life, and thus caused high maintenance costs. Therefore, it is important to study the corrosion mechanism of ships and the corrosion resistance of surface coatings. Electrochemical impedance spectroscopy (EIS) became one of the main methods to study and evaluate the coating metal system because it was an *in-situ* measurement of the electrochemical parameters related to the coating system performance and coating failure process, such as coating capacitance resistance, interface double layer capacitance, charge transfer resistance, etc. [31, 32].

After analyzing the EIS measurement results of the samples, the original data was fitted with Zview software (Version 3.1, Scribner Associates Inc., USA), and the Nyquist plots of four coatings and metal substrates were displayed in Fig 12. By analyzing the capacitive arc radius of each sample in the Nyquist plot, the corrosion resistance of the coatings could be intuitively compared. In the Nyquist diagram, the corrosion resistance of the coating was related to the radius of the capacitive reactance arc. The larger the radius was, the greater the resistance was, indicating that the corrosion resistance of the coating was stronger [33–35]. The red dotted line diagram was the original data, the blue was the fitting data, and the dotted line box was the fitting equivalent circuit diagram.

In Fig. 12, the capacitive arc radii of different samples greatly varied. The radius of bare Q235 was in the order of 10^2, which was the smallest among all samples. The radius of PDMS was 10^3 orders of magnitude. In contrast, the radii of three DIP coatings DISP, DIVP, and DIEP, were 10^8, 10^{11}, and 10^6 orders

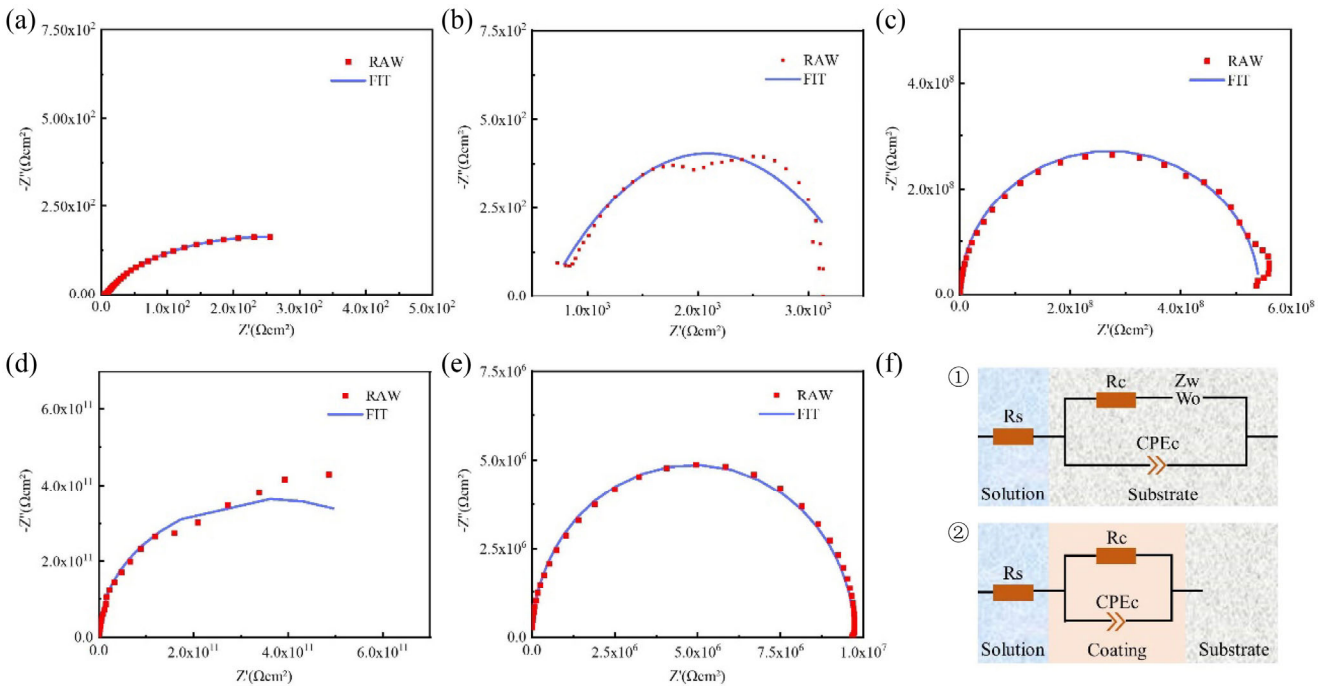

Fig. 12 Nyquist curves of (a) PDMS; (b) bare Q235 substrate; (c) DISP coating; (D) DIVP coating; and (e) DIEP coating. (f) Schematic diagram of the three-electrode system.

of magnitude, respectively, which were much larger than bare Q235 and PDMS and displayed excellent corrosion resistance. In each coating equivalent circuit, R_s was solution resistance, R_1 was interface transfer resistance, and C_{coat} was a constant phase angle element whose impedance was divided into two parts: real ($C_{coat\text{-}T}$) and imaginary ($C_{coat\text{-}P}$). The equivalent circuit parameter values of each sample are presented in Table 4. The value of R_1 also corresponded to the difference of the capacitive arc radius of each sample in Fig 12, indicating that the three polysaccharide coatings had strong corrosion resistance, and the cell wall polysaccharide coating had the best corrosion resistance.

EIS measurements were also employed to further investigate the anticorrosion characteristics of coatings. Figure 13 displayed the corresponding Bode modulus and Bode plots of phase angle, respectively. #1, #2, #3, #4, and #5 represented bare Q235, PDMS film, DISP, DIVP, and DIEP, respectively. Typically, the impedance values at a low measured frequency of 0.01 Hz ($|Z|_{0.01\,Hz}$) could better reflect the barrier properties of a coating system. The higher $|Z|_{0.01\,Hz}$ values meant better barrier properties. From #1 to #4, the $|Z|_{0.01\,Hz}$ was sharply increased from 10^2 Ω·cm^2 to 10^{11} Ω·cm^2, and then declined to 10^7 Ω·cm^2 of #5. The corrosive process occurred at the metal/solution interface for #1 (bare Q235) and #2 (PDMS film), while #3–#5 (DIP coatings) showed attractive corrosion protection performance, among whom the #4 (DIVP coating) investigated the best anticorrosion property. In Fig. 13(b), the phase angle plots of #3–#5 showed only one peak corresponding to one time constant. This indicated that the corrosive mediums did not arrive at the metal interface, and the coating still acted as a good barrier. Except for #3–#5, a second peak appeared in other plots at the low-frequency region, which illustrated that the second time constant showed up and those coatings showed different degrees of corrosion.

The Tafel curve is a portion of the polarization curve in the strongly polarized region. All Tafel polarization curves of various coatings are depicted in Fig. 14(a), and the parameters obtained from Tafel curves, such as corrosion potential (E_{corr}) and corrosion current density (i_{corr}), are summarized in Fig. 14 (b). According to the literature, the higher the E_{corr}, the better the corrosion resistance. The lower the i_{corr}, the slower the corrosion velocity [36, 37]. It could be seen from the figures that for all DIP coatings, the E_{corr} values were higher than Q235 substrate and PDMS coating, and #4 showed the highest corrosion potential

Table 4 Equivalent circuit parameter values.

Parameter	Q235	PDMS	DISP	DIVP	DIEP
R_s (Ω·cm^2)	5.21	625.3	1.96×10^4	2.20×10^9	3.89×10^3
$C_{coat\text{-}T}$ (F/cm^2)	3.00×10^{-3}	5.12×10^{-5}	1.02×10^{-11}	1.19×10^{-11}	8.76×10^{-12}
$C_{coat\text{-}P}$ (F/cm^2)	0.702	0.344	/	/	/
R_1 (Ω·cm^2)	0.61×10^3	2.92×10^3	5.43×10^8	6.93×10^{11}	9.72×10^6

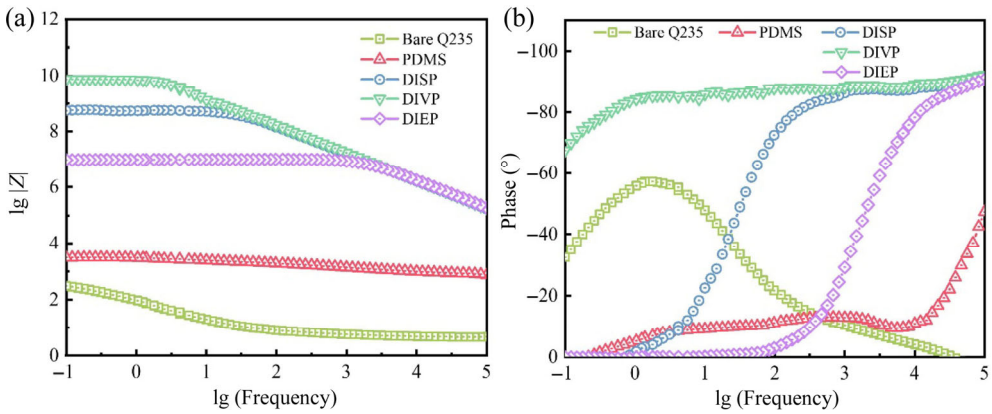

Fig. 13 (a) Bode modulus plots and (b) Bode phase angle plots of samples. The unit of Z is Ω·cm^2, and the unit of frequency is Hz.

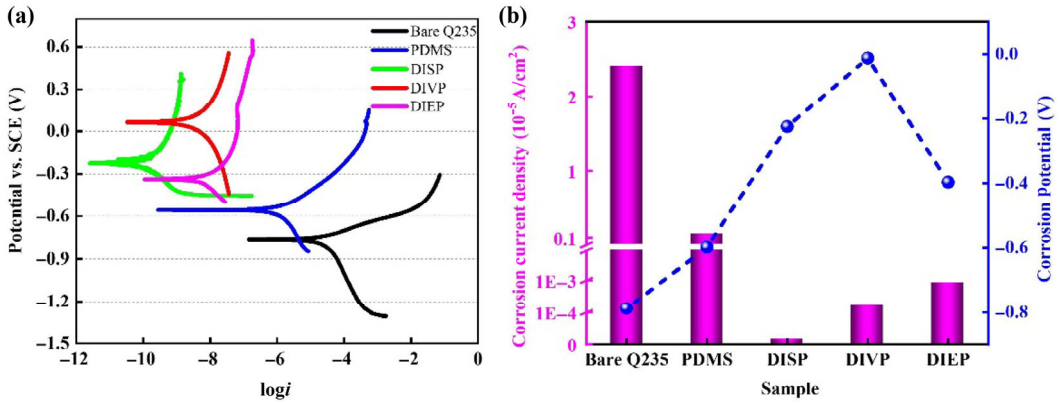

Fig. 14 (a) Tafel curves of all samples in 3.5 wt% NaCl solution; (b) electrochemical polarization measurement electrochemical parameters. SCE represents the saturated calomel electrode. i represents the current density (A/cm^2).

Table 5 i_{corr} and E_{corr} values.

Parameter	Q235	PDMS	DISP	DIVP	DIEP
i_{corr} (A/cm^2)	2.41×10^{-5}	1.40×10^{-6}	1.49×10^{-10}	2.89×10^{-9}	9.25×10^{-9}
E_{corr} (V)	−0.767	−0.558	−0.225	−0.012	−0.392

of −0.207 V. While the i_{corr} presented the converse tendency, showing that #4 exhibited the lowest corrosion current density of 2.89×10^{-9} A, which reduced 4 orders of magnitude compared to #1 (2.41×10^{-5} A). By contrast, it could be concluded that the DIVP coating showed the best corrosion resistance ability.

To explain different anticorrosion behaviors of samples, corrosion resistance mechanism diagrams were displayed in Fig. 15. The corrosion resistance of the coating was related to the stable and compact lubricating layer, which could be used as an excellent hydration barrier to prevent the penetration of corrosive media such as water, ions, and dissolved oxygen [29]. It could be seen from the infrared spectrum of the polysaccharide coating that the polysaccharide molecular chain contained many

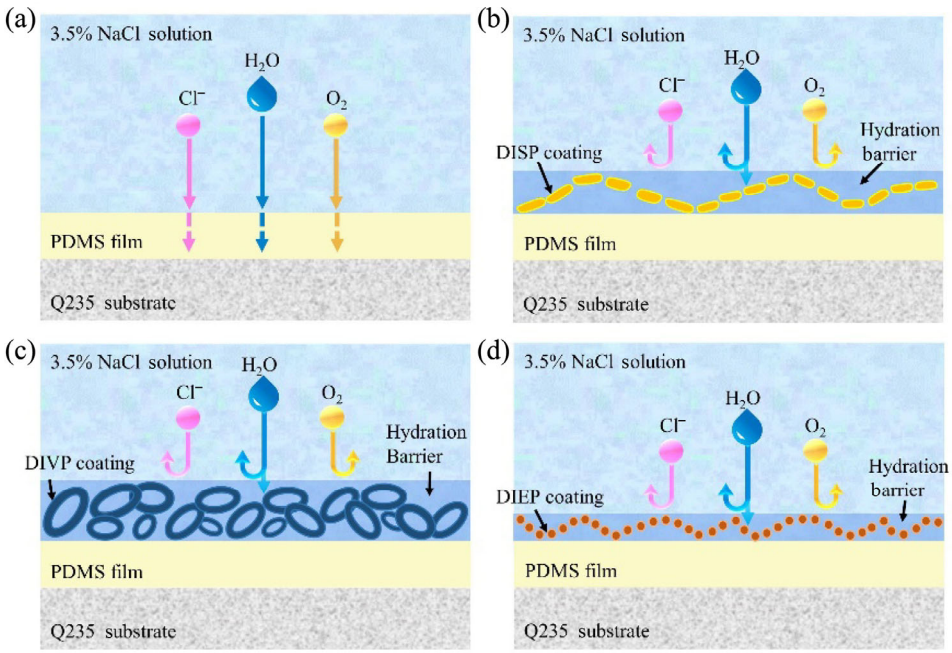

Fig. 15 Anticorrosion mechanism diagrams of the hydration barrier on different coatings.

hydrophilic functional groups, such as hydroxyl, etc. These hydrophilic groups would bond with the polar water molecules in the solution through chemical bonds to form a dense hydrated barrier. This would further prevent the corrosion medium from passing through the coating and play a role in corrosion prevention. The corrosion resistance was related to the thickness of the hydration barrier formed by polysaccharide molecules and water molecules. The thicker the barrier, the stronger the corrosion resistance.

3.4 Antifouling and self-cleaning performance

Antifouling performance of coatings is also a very important index for estimating the service property because of the great harm of fouling organisms to underwater equipment [38]. We investigated the resistance of the coatings against algal and other typical common dirt (water and oil-based stamp).

It is well-known that the most important step for forming marine fouling was the formation of biofilm, which provided nutrients for the offspring of large fouling organisms and greater adhesion for all kinds of microorganisms. Therefore, Chlorella, unicellular algae distributing worldwide, was selected to test the anti-adhesion ability. In Section 2.4, the Chlorella nutrition process was demonstrated. After immersing the samples in Chlorella solution for three days, surfaces were washed with water, and the morphological observation and measurement of Chlorella were performed using an inverted optical microscope (CKX53, Olympus, Japan) equipped with a digital camera and computer. Figure 16(a) displayed the morphological images of Chlorella adhesion on samples. It was obvious that simple PDMS could not withstand the fouling organisms inhibiting. On the contrary, the DIP coatings showed quite an anti-biofouling ability. In Fig. 16(b), the colonized Chlorella per region on the surfaces was counted. It was quite obvious that there was an order of magnitude difference in the attachment density of Chlorella between DIP coatings and PDMS. Compared to bare PDMS, DISP, DIVP, and DIEP behaved 4.8, 24.1, and 9.2 times antifouling performance, revealing that DIVP coating behaved the best. At the same time, in order to verify the antifouling durability of DIP

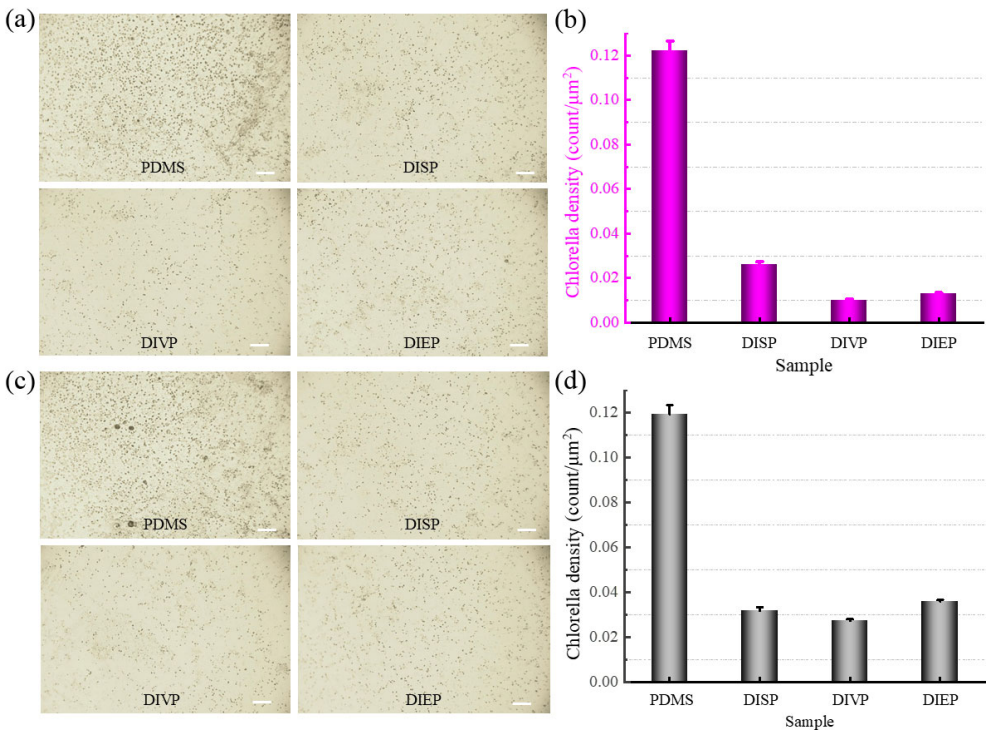

Fig. 16 (a) Test about inhibition of Chlorella attachment, (b) histogram of Chlorella density on coating surfaces on the samples just prepared; (c) the observation of Chlorella attachment, and (d) histogram of Chlorella density on the surfaces after being immersed in flowing water. All scale bars are 10 μm

coatings, samples were immersed in flowing water. After one week, all samples were subjected to the Chlorella adhesion test again, and the observation results of surfaces are displayed in Figs. 16(c) and 16(d). Compared to bare PDMS, DISP, DIVP, and DIEP behaved 3.6, 4.5, and 3.1 times antifouling performance, proving the antifouling durability of DIP coatings.

The bio-antifouling mechanism of the hydrophilic surface differed from that of the hydrophobic surface, and it was easy to form hydrogen bonds, electrostatic induction, or chemical bonding hydrate barrier layer on the hydrophilic surface. When fouling organisms attached to the surface, the hydration barrier increased the energy loss when water drops rolled off, thus providing a physical barrier for the surface to resist the fouling organism's adhesion [16], and its antifouling mechanism was consistent with that in Fig. 15. This mechanism indicated that the hydrophilic surface could resist the initial process of biological fouling [39].

The DIP coatings were also proven with excellent antifouling properties for inorganic pollutants. The seal stains and cleaning tests were conducted on the coatings with water-based and oil-based stamps to further verify the antifouling effect of the samples. In Fig. 17(a1), PDMS was stamped with oil-based ink,

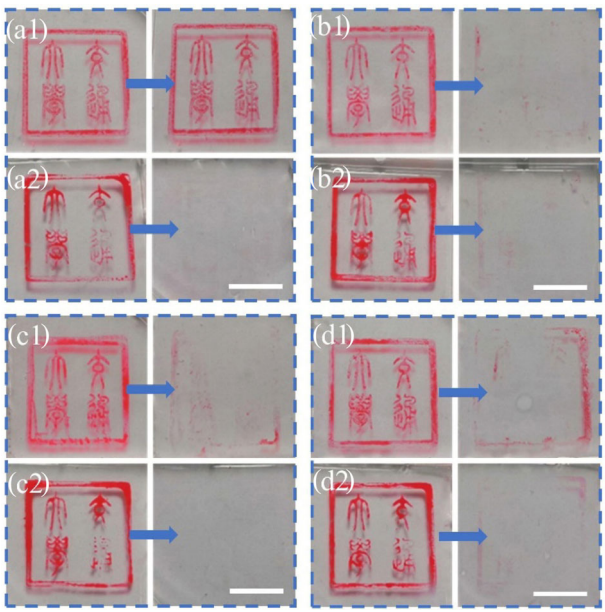

Fig. 17 Imprint and removal of oil-based stamps on (a1) PDMS, (b1) DISP coating, (c1) DIVP coating, (d1) DIEP coating and water-based stamps on (a2) PDMS, (b2) DISP coating, (c2) DIVP coating; (d2) DIEP coating. All scale bars are 1 cm.

and the pattern "交通大学" could be observed. Then, the pattern was washed with water for 30 s, but the mark was still visible. The same pattern with a water-based stamp was deposited on PDMS. However, the words were completely wiped (Fig. 17(a2)), owing to PDMS's lipophilic and hydrophobic characteristics. On the surface of DIP coatings, better decontamination ability was still observed for water-based or oil-based stamps than PDMS. Even though the three DIPs were hydrophilic, the water-based pollutant could still be washed on the surface by running water.

After the above experimental verification, DIP coatings demonstrated excellent antifouling performance in the face of organic and inorganic adhesion. These contaminants could also be easily removed by water flow, owing to the hydration barrier acting as a physical barrier for the resistance of the surface against fouling adhesion [40].

4 Conclusions

The work proposed a facile and novel method of fabricating coatings with antifouling and anticorrosion performance and slippery and drag-reducing behavior. Three different coatings (DISP, DIVP, and DIEP) were deposited on PDMS film to cover and protect the metal substrate. The experimental results were as follows:

1) Compared to the simple PDMS film, PDMS covered with DIP coatings showed ultra-low COF. The coatings reduced the COF from 1.082 to below 0.025.

2) PDMS covered with the DIP coatings showed drag reduction performance (2%–6%). The DISP sample investigated the best drag reduction, with a maximum of 5.72%.

3) Compared to the reference groups (bare Q235 and PDMS), DIP coatings showed great antifouling and anticorrosion performance. These performances were attributed to the functionality of the hydration barrier, whose presence effectively reduced the adhesion of contaminants and isolated the exchange of ions and water between the solution and the protected substrate.

We foresee that the environmental-friendly DIP coatings could have broad applications in marine equipment, where they could significantly save energy,

cost, and labor in cleaning and maintaining underwater surfaces.

Acknowledgements

The authors acknowledge the National Natural Science Foundation of China (52375298, 51975458, and 51905370), the financial support from the China Scholarship Council, China Postdoctoral Science Foundation funded project (2020M673377 and 2020T130510), Key R&D program of Shaanxi Province (2022SF-069) and the Natural Science Fund of Shaanxi Province (2020JM-010). The authors would like to thank the instrument analysis center of Xi'an Jiaotong University for their assistance with SEM and AFM analysis.

Declaration of competing interest

The authors have no competing interests to declare that are relevant to the content of this article.

References

[1] Gokulakrishnan S A, Arthanareeswaran G, László Z, Veréb G, Kertész S, Kweon J. Recent development of photocatalytic nanomaterials in mixed matrix membrane for emerging pollutants and fouling control, membrane cleaning process. *Chemosphere* **281**: 130891 (2021)

[2] Han X, Wu J H, Zhang X H, Shi J Y, Wei J X, Yang Y, Wu B, Feng Y H. Special issue on advanced corrosion-resistance materials and emerging applications. The progress on antifouling organic coating: From biocide to biomimetic surface. *J Mater Sci Technol* **61**: 46–62 (2021)

[3] Jin H C, Tian L M, Bing W, Zhao J, Ren L Q. Bioinspired marine antifouling coatings: Status, prospects, and future. *Prog Mater Sci* **124**: 100889 (2022)

[4] Amara I, Miled W, Ben Slama R, Ladhari N. Antifouling processes and toxicity effects of antifouling paints on marine environment. A review. *Environ Toxicol Pharmacol* **57**: 115–130 (2018)

[5] Fan X Q, Song S J, Shi Y T, Cai M, Huang Y, Zhang B B, Zhu M H. Mechanochemical stable superhydrophobic coating toward lasting corrosion protection. *Prog Org Coat* **178**: 107478 (2023)

[6] Wong T S, Kang S H, Tang S K Y, Smythe E J, Hatton B D, Grinthal A, Aizenberg J. Bioinspired self-repairing slippery surfaces with pressure-stable omniphobicity. *Nature* **477**(7365): 443–447 (2011)

[7] Amini S, Kolle S, Petrone L, Ahanotu O, Sunny S, Sutanto C N, Hoon S, Cohen L, Weaver J C, Aizenberg J, et al. Preventing mussel adhesion using lubricant-infused materials. *Science* **357**(6352): 668–673 (2017)

[8] Yin J L, Mei M L, Li Q L, Xia R, Zhang Z H, Chu C H. Self-cleaning and antibiofouling enamel surface by slippery liquid-infused technique. *Sci Rep* **6**: 25924 (2016)

[9] Yuan S C, Lin D, Zhang X G, Wang H Y. Fabrication and application of Slippery Liquid Infused Porous functional surface. *Prog Chem* **33**(1): 87–96 (2021)

[10] Basu S, Hanh B M, Isaiah Chua J Q, Daniel D, Ismail M H, Marchioro M, Amini S, Rice S A, Miserez A. Green biolubricant infused slippery surfaces to combat marine biofouling. *J Colloid Interface Sci* **568**: 185–197 (2020)

[11] Qin L G, Yang H, Mawignon F J, Zhang Y L, Dong G N. A facile method for fabricating super-slippery surface with long term and high-efficiency sustained release performance. *Prog Org Coat* **174**: 107275 (2023)

[12] Zhai G Z, Qi L X, He W, Dai J J, Xu Y, Zheng Y M, Huang J L, Sun D H. Durable super-hydrophobic PDMS@SiO_2@WS_2 sponge for efficient oil/water separation in complex marine environment. *Environ Pollut* **269**: 116118 (2021)

[13] Park S, Park J, Heo J, Lee S E, Shin J W, Chang M, Hong J. Polysaccharide-based superhydrophilic coatings with antibacterial and anti-inflammatory agent-delivering capabilities for ophthalmic applications. *J Ind Eng Chem* **68**: 229–237 (2018)

[14] Wang Y L, Lai L, Teng L P, Li Y H, Cheng J Q, Chen J H, Deng C. Mechanism of the anti-inflammatory activity by a polysaccharide from *Dictyophora indusiata* in lipopolysaccharide-stimulated macrophages. *Int J Biol Macromol* **126**: 1158–1166 (2019)

[15] Pradal C, Yakubov G E, Williams M A K, McGuckin M A, Stokes J R. Responsive polysaccharide-grafted surfaces for biotribological applications. *Biotribology* **18**: 100092 (2019)

[16] McNamee C E, Yamamoto S, Kappl M, Butt H J, Higashitani K, Dėdinaitė A, Claesson P M. Surface and friction forces between grafted polysaccharide layers in the absence and presence of surfactant. *J Colloid Interface Sci* **364**(2): 351–358 (2011)

[17] Bourouis I, Pang Z H, Liu X Q. Recent advances on uses of protein and/or polysaccharide as fat replacers: Textural and tribological perspectives: A review. *J Agric Food Res* **11**: 100519 (2023)

[18] Ji L, den Otter D, Cornacchia L, Sala G, Scholten E. Role of polysaccharides in tribological and sensory properties of model dairy beverages. *Food Hydrocoll* **134**: 108065 (2023)

[19] Bigot S, Louarn G, Kébir N, Burel F. Click grafting of seaweed polysaccharides onto PVC surfaces using an ionic liquid as solvent and catalyst. *Carbohydr Polym* **98**(2): 1644–1649 (2013)

[20] Zou B Q, Zhou C, Xu L X, Wan R, Hu F X, Guo S J. Scale effect of applying Tauti's law in model experiment: CFD models for flow across planar netting. *Ocean Eng* **256**: 111552 (2022)

[21] Li X R, Li J, Wang J Y, Yuan J, Jiang F, Yu X Y, Xiao F P. Recent applications and developments of polyurethane materials in pavement engineering. *Constr Build Mater* **304**: 124639 (2021)

[22] Ma Z Y, Liu J B, Zhang X D, Deng R X, Lu S, Wu Y H, Qin L G, Dong G N. Flexible surfaces prepared through direct ink writing with drag reduction and antifouling. *Colloids Surf A Physicochem Eng Aspects* **655**: 130233 (2022)

[23] Vaitkunaite G, Espejo C, Thiebaut B, Neville A, Morina A. Low friction tribofilm formation and distribution on an engine cylinder tested with MoDTC-containing low viscosity engine lubricants. *Tribol Int* **171**: 107551 (2022)

[24] Ma Z Y, Huang R X, Kostyantyn G, Wang Y, Li R T, Liu Z Q, Xu J J. Tribology properties of titanium-based metals reinforced by BN nanosheets. *Adv Eng Mater* **23**(8): 2001351 (2021)

[25] Berger S, Müller E, Schnabelrauch M. Influence of methacrylate-containing surface modifiers on the mechanical properties of nano-hydroxyapatite/polylactide network composites. *Mater Lett* **63**(30): 2714–2717 (2009)

[26] Javed M A, Ang A S M, Bhadra C M, Piola R, Neil W C, Berndt C C, Leigh M, Howse H, Wade S A. Corrosion and mechanical performance of HVOF WC-based coatings with alloyed nickel binder for use in marine hydraulic applications. *Surf Coat Technol* **418**: 127239 (2021)

[27] Wang Y, Li Q Z, Shao T R, Miao W J, You C, Wang Z B. Fabrication of anti-fouling and anti-bacterial hydrophilic coating through enzymatically-synthesized cellooligomers. *Appl Surf Sci* **600**: 154133 (2022)

[28] Zhang L H, Peng X Y, Liu Z F, Wei N X, Wang F. An application of augmented Lagrangian differential evolution algorithm for optimizing the speed of inland ships sailing on the Yangtze River. *Int J Nav Archit Ocean Eng* **14**: 100488 (2022)

[29] Yang Z C, He X Y, Chang J F, Yuan C Q, Bai X Q. Facile fabrication of fluorine-free slippery lubricant-infused cerium stearate surfaces for marine antifouling and anticorrosion application. *Surf Coat Technol* **415**: 127136 (2021)

[30] Davies J, Truong-Ba H, Cholette M E, Will G. Optimal inspections and maintenance planning for anti-corrosion coating failure on ships using non-homogeneous Poisson Processes. *Ocean Eng* **238**: 109695 (2021)

[31] Hussain A K, Seetharamaiah N, Pichumani M, Chakra C S. Research progress in organic zinc rich primer coatings for cathodic protection of metals—A comprehensive review. *Prog Org Coat* **153**: 106040 (2021)

[32] Cai M, Feng P, Yan H, Li Y T, Song S J, Li W, Li H, Fan X Q, Zhu M H. Hierarchical $Ti_3C_2T_x$@MoS_2 heterostructures: A first principles calculation and application in corrosion/wear protection. *J Mater Sci Technol* **116**: 151–160 (2022)

[33] Wu Y M, Zhao W J, Qiang Y J, Chen Z J, Wang L P, Gao X L, Fang Z W. π–π interaction between fluorinated reduced graphene oxide and acridizinium ionic liquid: Synthesis and anti-corrosion application. *Carbon* **159**: 292–302 (2020)

[34] Yan H, Fan X Q, Cai M, Song S J, Zhu M H. Amino-functionalized $Ti_3C_2T_x$ loading ZIF-8 nanocontainer@ benzotriazole as multifunctional composite filler towards self-healing epoxy coating. *J Colloid Interface Sci* **602**: 131–145 (2021)

[35] Fan X Q, Yan H, Cai M, Song S J, Huang Y, Zhu M H. Achieving parallelly-arranged $Ti_3C_2T_x$ in epoxy coating for anti-corrosive/wear high-efficiency protection. *Compos Part B Eng* **231**: 109581 (2022)

[36] Ramirez-Soria E H, León-Silva U, Lara-Ceniceros T E, Bazán-Díaz L, Advíncula R C, Bonilla-Cruz J. Graphene oxide bifunctionalized with NH_2/NH_3^+ and their outstanding-performance against corrosion. *Appl Surf Sci* **561**: 150048 (2021)

[37] Thongchuea N, Warinsiriruk E, Phuraya N, Sa-Ngasoongsong P. (2020) Corrosion behavior on cerclage-wire joining using laser welding. In: Proceedings of the 2nd materials research society of thailand international conference, Pattaya, Thailand, 2020: 080002.

[38] Dong W R, Li B C, Wei J F, Tian N, Liang W D, Zhang J P. Environmentally friendly, durable and transparent anti-fouling coatings applicable onto various substrates. *J Colloid Interface Sci* **591**: 429–439 (2021)

[39] Cao N, Jiang R J, Hao L W, Tian L M, Mo R, Fan Y, Zhao J, Ren L Q. Anti-adhesive and bactericidal polymeric coating based on Schiff-base reaction. *Mater Lett* **250**: 182–185 (2019)

[40] Sarker P, Chen G T, Sajib M S J, Jones N W, Wei T. Hydration and antibiofouling of TMAO-derived zwitterionic polymers surfaces studied with atomistic molecular dynamics simulations. *Colloids Surf A Physicochem Eng Aspects* **653**: 129943 (2022)

Hao YANG. He received his bachelor's degree in mechanical engineering in 2017 from Xi'an Jiaotong University, China. After then, he is a Ph.D. student in the Key Laboratory of Education Ministry for Modern Design & Rotor Bearing System at the same university. His research interests include surface drag reduction technology (pollution protection and surface drag reduction design for marine equipment) and the design of functional surfaces (design and manufacturing of flexible, intelligent, and micro nano surfaces).

Liguo QIN. He currently holds associate professor in Xi'an Jiaotong University, China. His research work is on how to control the tribological performance of engineering surface and how the surface interacts with lubricants. The aim is to solve problems and generate greater understanding relevant to a range of applications including bio-tribology, drag reduction & multifunctional surface construction. He has published papers over 40 in related journals, such as *Applied Surface Science*, *Tribology International*, and *Carbohydrate Polymers*. He obtained the university excellent doctoral thesis and Shaanxi province excellent doctoral thesis (2018), and was invited over 10 times speaking. During European Advanced Materials Congress of 2018, he was awarded IAAM Scientist Medal. As the principle investigator, he hosted 10 projects including National Natural Science Foundation of China, Natural Science Fund of Shaanxi Province and China Postdoctoral Science Foundation funded project.

Yali ZHANG. She is a full professor in the School of Life Science and Technology at Xi'an Jiaotong University, China. She achieved her M.S. degree (2001) in organic chemistry from Shaanxi Normal University, China. She completed her Ph.D. degree in biomedical engineering at Xi'an Jiaotong University in 2010, and then served as a professor at the School of Life Science and Technology, Xi'an Jiaotong University. During 2013–2014, she worked as a research fellow at University of Illinois, USA. Her current research interest lies in the biochemistry and molecular biology, with a focus on glycobiology, and the functional research of natural products.